JACS
JOURNAL OF THE AMERICAN CHEMICAL SOCIETY
Article
Cite This: J. Am. Chem. Soc. 2019, 141, 4749−4755
pubs.acs.org/JACS

Cation-based Structural Tuning of Pyridine Dipyrrolate Cages and Morphological Control over Their Self-assembly

Huacheng Zhang,[†,‡] Juhoon Lee,[‡] James T. Brewster II,[‡] Xiaodong Chi,[‡] Vincent M. Lynch,[‡] and Jonathan L. Sessler*[,‡,§]

[†]School of Chemical Engineering and Technology, Xi'an Jiaotong University, Xi'an, Shaanxi 710049, China
[‡]Department of Chemistry, The University of Texas at Austin, Austin, Texas 78712-1224, United States
[§]Institute for Supramolecular and Catalytic Chemistry, Shanghai University, Shanghai 200444, China

* Supporting Information

ABSTRACT: Different pyridine dipyrrolate cages including cage-based dimers and polymers may be fabricated in a controlled manner from the same two starting materials, namely, an angular ligand 1 and $Zn(acac)_2$, by changing the counter cation source. With tetrabutylammonium (TBA^+) and dimethyl viologen (DMV^{2+}), Cage-3 and Cage-5 are produced. In these cages, two ligands act as bridges and serve to connect together two cage subunits to produce higher order ensembles. In Cage-3 and Cage-5, the TBA^+ and DMV^{2+} counter cations lie outside the cavities of the respective cages. This stands in contrast to what is seen with a previously reported Cage-1, wherein dimethylammonium (DMA^+) counter cations reside within the cage cavity. When the counter cations are tetraethylammonium (TEA^+) and bis(cyclopentadienyl) cobalt(III) (Cp_2Co^+), polymeric cage materials, PC-1 and PC-2, are formed, respectively. The counter cations thus serve not only to balance charge but also to tune the structural features as a whole. The organic cations used in the present study also act to modulate the further assembly of individual cages. The present cation-based tuning emerges as a new method for a fine-tuning of the multidimensional morphology of self-assembled inorganic materials.

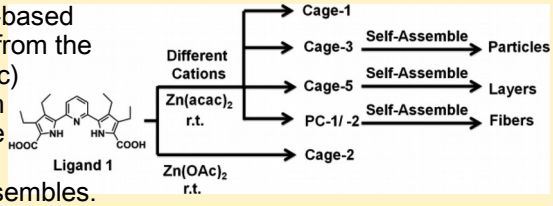

INTRODUCTION

Structure and morphology play key roles in defining the properties of nanomaterials, and control over these features is essential for effective manufacturing processes.[1] Understanding the underlying determinants is important from both the fundamental science[2] and applied engineering[3] perspectives. Not surprisingly, explorations of efficient morphological control methods have been the focus of considerable academic effort in recent years.[4] Self-assembly[5] has received particular attention in this regard. This latter approach has been used, for instance, to create mixed inorganic−organic supramolecular structures,[6,7] including metal-linked three-dimensional cages[6−8] that have attracted attention for their ability to recognize both neutral and charged[9,10] guests and to function as nanoscale reaction vessels.[11] Here, we report the use of different organic cations with various sizes and charges as a means of tuning the nature of the cage structures created from pyridine dipyrrolate and $Zn(acac)_2$, as well as the morphologies of various self-assembled constructs (particles, linear structures, and layers) formed from these cages.

We recently reported the preparation of zinc-directed self-assembled pyridine-dipyrrolate cages (Cage-1 and Cage-2) by using an inherently nonlinear ligand, pyridine-dipyrrolate 1 in conjunction with a Zn^{2+} cation source.[12] In both Cage-1 and Cage-2 (Scheme 1a), a hydroxide anion serves to bridge two constituent zinc dimers. The presence of these hydroxide bridges requires charge balance. In Cage-2, this charge balance is provided by the zinc ions, which are present in stoichiometric excess relative to the acetate anions present in the starting zinc salt (i.e., $Zn(OAc)_2$). However, in the case of Cage-1, where $Zn(acac)_2$ was used as the Zn^{2+} cation source, charge balance is provided by dimethylammonium (DMA^+) cations trapped inside the structure of Cage-1. These structural differences led us to consider that the DMA^+ cation in Cage-1 could be replaced[13] by other organic cations and that this replacement might provide a means of tuning not only structures of the Zn(II)-based cages but also how they interact with one another under conditions of self-assembly. To the extent this proved true, it would allow different inorganic−organic supramolecular products, as well as various morphological nanomaterials, to be accessed from the same exact precursors, namely, ligand 1 and $Zn(acac)_2$.

RESULTS AND DISCUSSION

Spectra Studies and Preparation of Metal Ion-directed Assemblies. To test the above possibility, we chose to mix ligand 1 with $Zn(acac)_2$ in DMF−methanol solution (1/4, v/v) in the presence of representative organic cations with different sizes and charges, namely, tetraethylammonium (TEA^+), tetrabutylammonium (TBA^+), bis(cyclopentadienyl) cobalt(III) (Cp_2Co^+), and dimethyl

Received: January 28, 2019
Published: February 27, 2019

DOI: 10.1021/jacs.9b01042
J. Am. Chem. Soc. 2019, 141, 4749−4755

Scheme 1. Structural Formulas of Pyridine-dipyrrolate 1, $Zn(OAc)_2$-Directed Cage-2, $Zn(acac)_2$-Directed Cage Dimers Cage-1, Cage-3, and Cage-5, Charge Balanced with DMA^+, TBA^+, and DMV^{2+}, Respectively, and $Zn(acac)_2$-Directed Polymeric Cages PC-1 and PC-2, Charge Balanced with TEA^+ and Cp_2Co^+, Respectively[a]

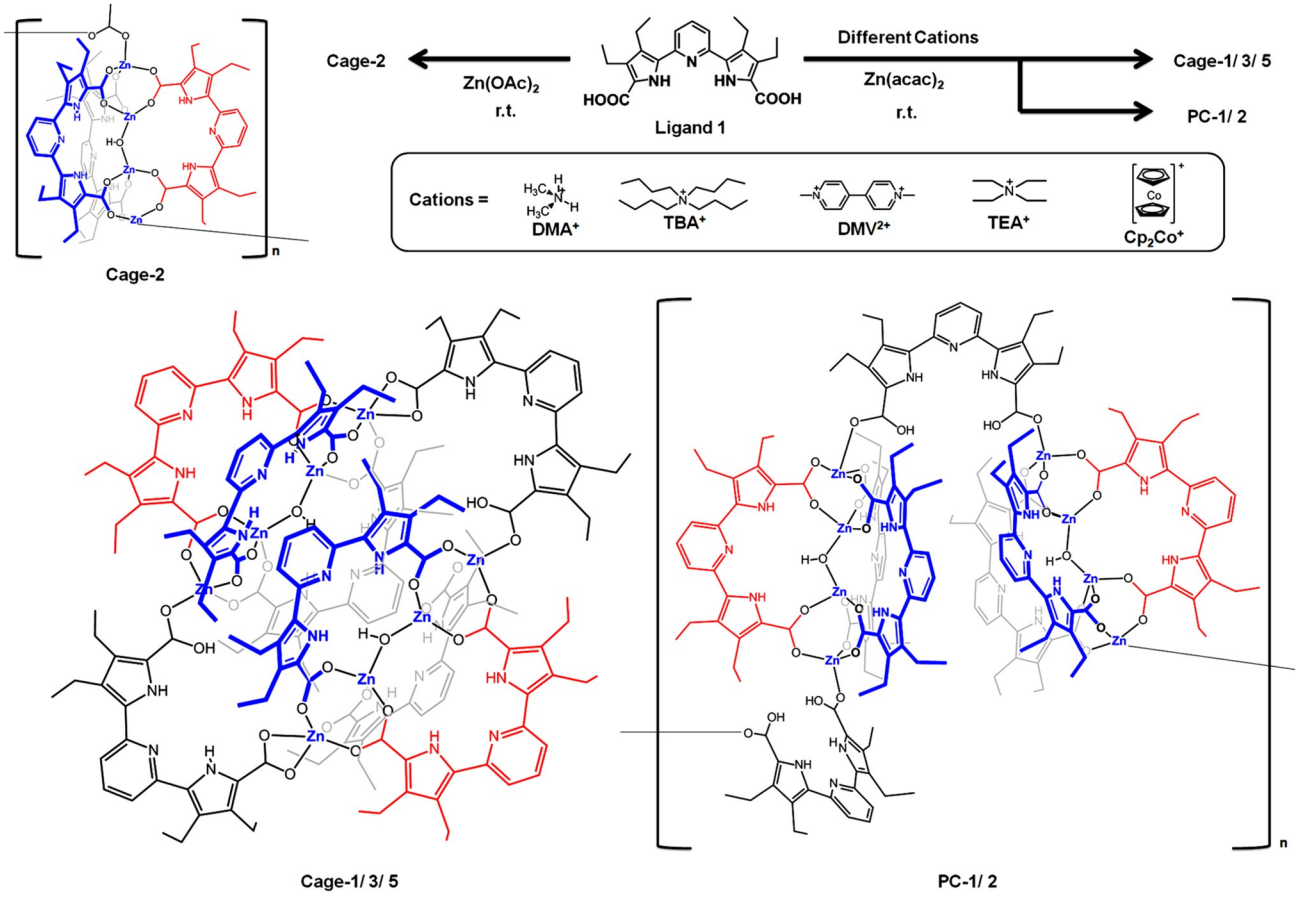

[a]The different subunits of 1 in the chemical structure are labeled in blue, red, grey, and black, respectively.

viologen (DMV^{2+}, Scheme 1). All cations were studied as their PF_6^- salts; however, the TEA^+ and TBA^+ cations were further studied in the form of other salts (i.e., containing a range of different counteranions; cf. Table S1). Upon mixing, an immediate change from colorless to pink was seen in the solutions containing DMV^{2+}, ligand 1, and $Zn(acac)_2$. Furthermore, compared to a pure solution of ligand 1 in this same solvent mixture, blue shifts in the so-called R band (around 270−300 nm) in the UV spectrum (Figure S1), red shifts in the emission maxima in the fluorescent spectra (Figure S2), and upfield shifts in the pyridine proton resonances of ligand 1 in the ^1H NMR spectra (Figure S3) are seen upon exposure to Zn(II). This was taken as preliminary evidence that metal ion-directed assemblies are being formed upon mixing.

To obtain detailed structural information, the self-assembly reactions were carried out under conditions analogous to those used previously to produce single crystals of Cage-1 but in the presence of various cation salts. Specifically, hexanes were allowed to vapor diffuse into mixed solutions of DMF and methanol (1/4, v/v) containing ligand 1, $Zn(acac)_2$, and different cationic salts at room temperature (Table S1 and the X-ray Experimental Section in the Supporting Information).

Cation-based Structural Tuning of Dimeric and Polymeric Cages. As inferred from single crystal X-ray crystallographic analyses, cage-like architectures, namely, Cage-3 and Cage-5 (Figure 1), were obtained when salts of the relatively bulky cations TBA^+ and DMV^{2+}, were used. These cage systems bear superficial structural analogy to Cage-1 (Figure S4). For instance, two molecules of compound 1 act as bridging units to connect two individual cage subunits. However, in contrast to what is seen in Cage-1, wherein an encapsulated DMA^+ cation is observed, in Cage-3 (Figure S5) and Cage-5 (Figure S6) the TBA^+ and DMV^{2+} cations sit outside of the central cage-like cavities. Additionally, one molar equivalent of DMV^{2+} is present in the case of Cage-5, whereas two molar equivalents of TBA^+ and DMA^+ are found in the case of Cage-3 and Cage-1, respectively. This reflects charge balance.

Further studies of these single crystalline structures indicate that Cages-1, -3, and -5 differ in terms of their metric parameters (Table S2). These differences include the spacings between the zinc dimers (Figure S7), the dihedral angle between the two opposing pyridines ($\angle_{cages}$, Figure S8), the distance between these two pyridines (d, Figure S9), and the distance between two zinc atoms contained within two parallel zinc dimers (d_{Zn}, Figure S10).

Solvent molecules are present inside and outside of both Cage-3 (Figure S11) and Cage-5 (Figure S12). Presumably, these solvents play an important role in stabilizing and shaping these dimeric cage architectures (Figure S13), e.g., solvent

DOI: 10.1021/jacs.9b01042
J. Am. Chem. Soc. 2019, 141, 4749−4755

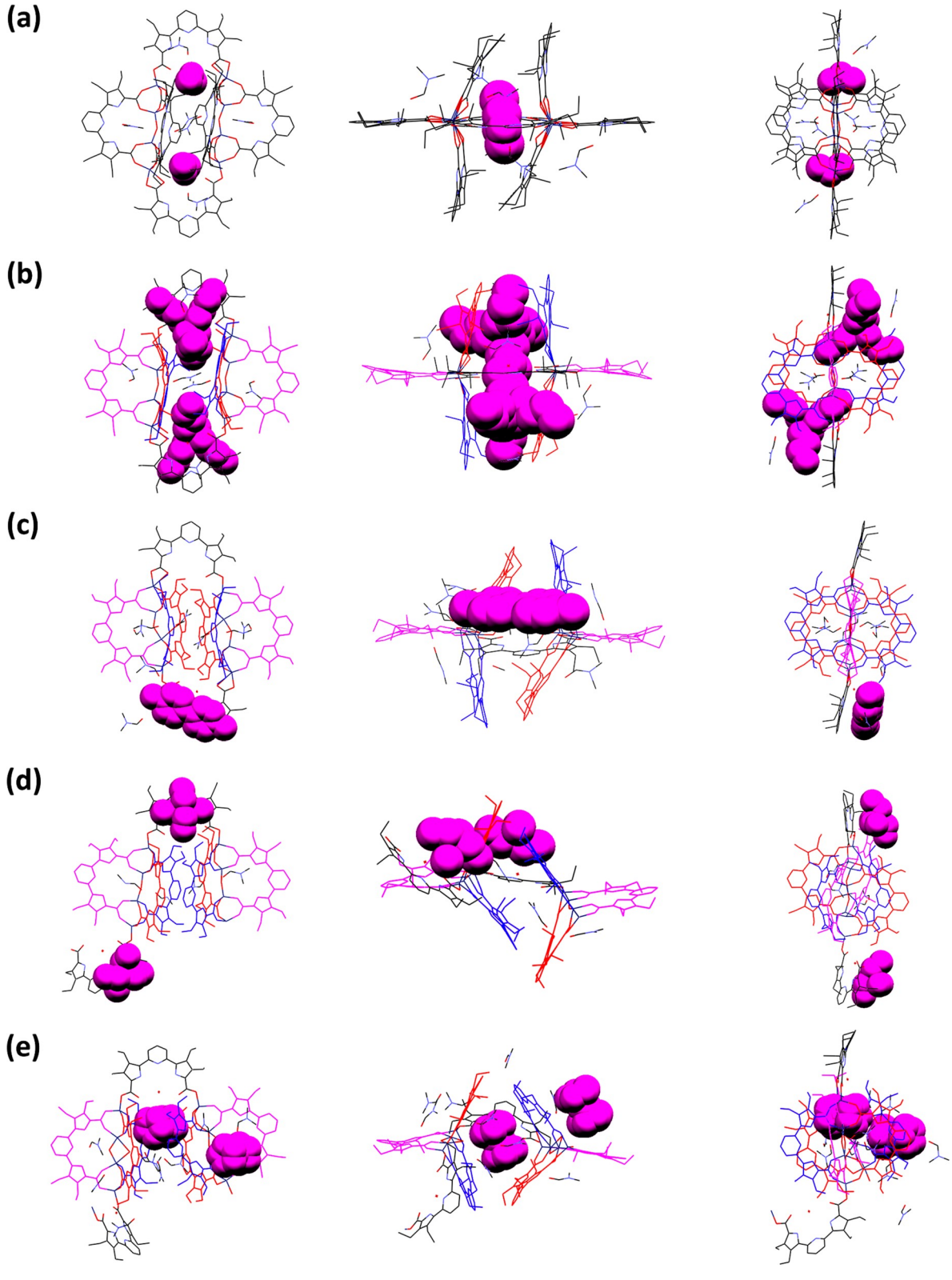

Figure 1. Crystal structures of Cage-1 (a), Cage-3 (b), Cage-5 (c), PC-1 (d), and PC-2 (e) viewed from front (left), top (middle), and side (right) in wireframe representations. Cations labeled in magenta are in space-filling representations. The different subunits of 1 in the structure are la using blue, red, magenta, and CPK coding, respectively. Hydrogen atoms are omitted for clarity.

molecules occupy the central cavities and are held in place through presumed hydrogen bonding interactions. The DMF molecules inside Cage-5 appear bound to the zinc centers (Figure S7 and Table S3) and likely serve to prevent the intrusion of the DMH_2^+ cation into the cage. In the solid state, solvent molecules outside the dimeric Cages-1, -3, and -5 act as "lids" that trap cations in gaps between the cages (Figure S14), as has been seen previously in other systems.[14]

DOI: 10.1021/jacs.9b01042
J. Am. Chem. Soc. 2019, 141, 4749−4755

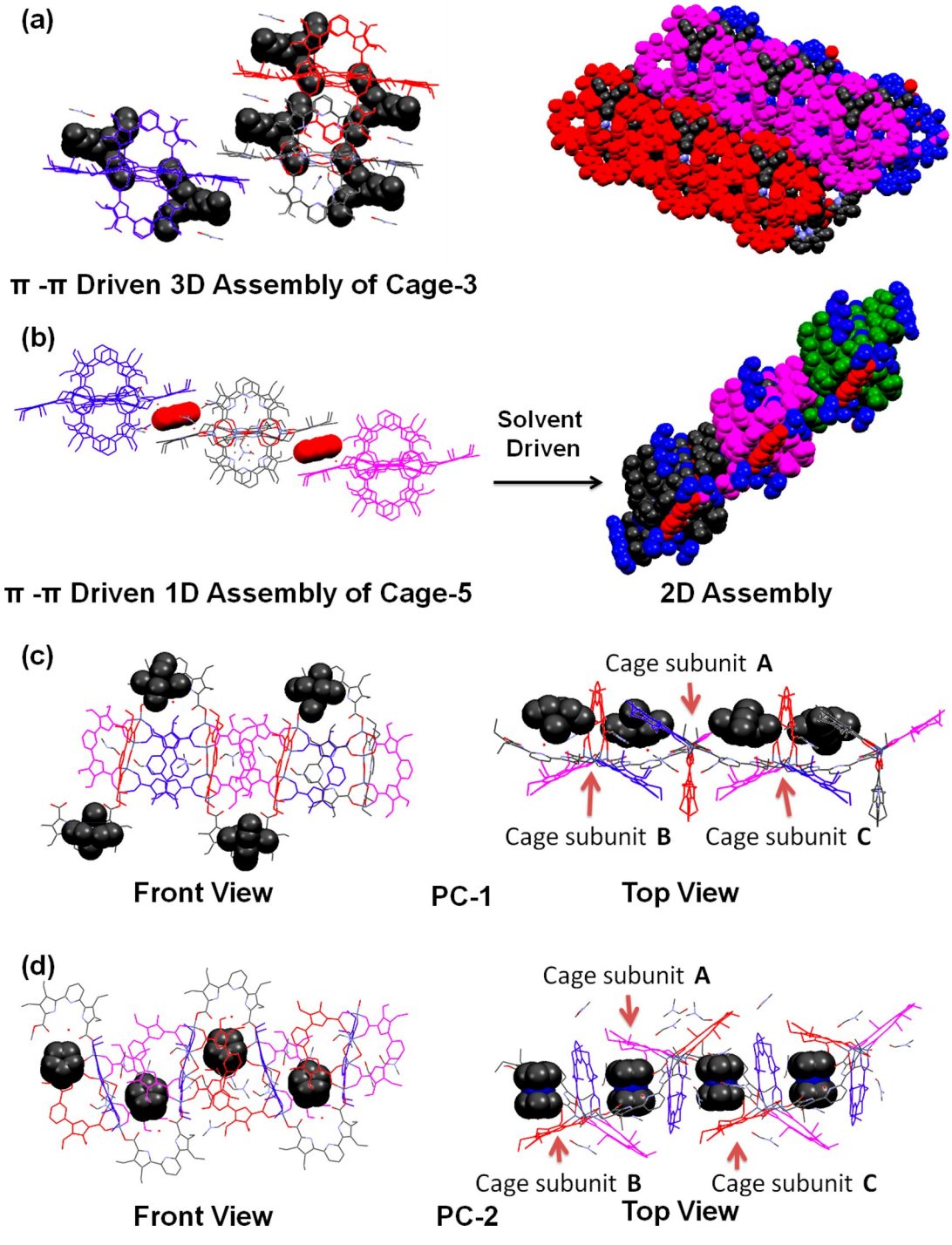

Figure 2. Front views of the single crystal X-ray diffraction structures of Cage-3 (a) and Cage-5 (b) showing the extended packing present in t solid state. Three-dimensional assemblies of Cage-3 driven by presumed π−π interactions are shown in truncated form (i.e., three repeat unit and in wireframe representations (2 repeat units; right) in space-filling representations. One-dimensional assemblies of Cage-5 driven by presumed π−π interactions, as well as further solvent-driven 2D assemblies of Cage-5 shown in wireframe representations (three repeat units and space-filling representations (nine repeat units; right), respectively. Individual units of ligand 1 are labeled in magenta, blue, and standard CPK coding. Crystal structures of two units of the infinite polymeric structures referred to as PC-1 (c) and PC-2 (d) in wireframe representations viewed from the front and top in wireframe representations. The different subunits of 1 in the structure are labeled using cyan, magenta, and CPK coding, respectively. Cations labeled in CPK coding are shown in space-filling representations. Hydrogen atoms are omitted for clarity.

By design, the relatively small cations Cp_2Co^+ and TEA^+ were selected to provide a range of sizes intermediate between those provided by DMA^+ and TBA^+. When ligand 1 and $Zn(acac)_2$ were mixed in the presence of TEA^+ and Cp_2Co^+, one-dimensional abacus-like cage polymers, PC-1 and PC-2 (Figure 1), were obtained as inferred from X-ray diffraction analyses. These polymeric cages share the same chemical structure, and both contain individual zinc dimer cage subunits wherein ligand 1 acts as linker (subunits of ligand 1 are labeled in black in Scheme 1). However, their crystalline structural arrangements are totally different, particularly with regard to the location of the various cations. For example, two molar

DOI: 10.1021/jacs.9b01042
J. Am. Chem. Soc. 2019, 141, 4749−4755

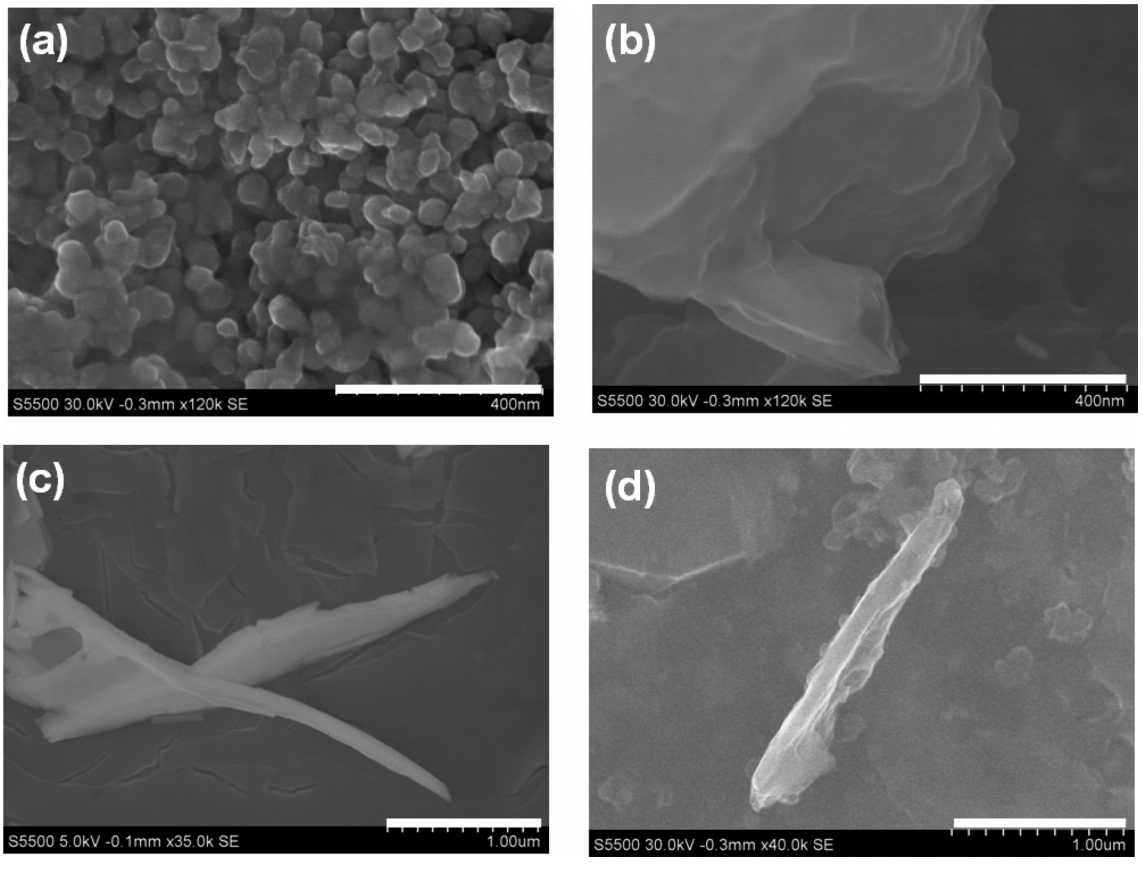

Figure 3. SEM images (d, scale bar = 400 nm; f, scale bar = 1 μm) obtained from solution samples prepared from combinations of $Zn(acac)_2$ and TBA^+ (1 mM), DMV^{2+} (1 mM), TEA^+ (1 mM), or Cp_2Co^+ (1 mM). All samples were prepared in a 1/4 (v/v) mixture of DMF and methanol.

equivalents TEA^+ are localized near the bridging ligands 1 and provide charge balance in the case of polymer PC-1 (Figure S15). In contrast, in PC-2 the Cp_2Co^+ cations slip into the cavities formed between two neighboring cage subunits (Figure S16).

Further studies of cation effects led to the conclusion that relatively small cations, such as DMA^+ and Cp_2Co^+, not only act as templates but then remain inside the cavities that are produced upon cage formation (Figure S17). This leads to a face-to-face orientation between nearby cage subunits (i.e., subunits A, B, and C in Figure 2), as well as the possibility of forming either infinite polymeric cage-containing structures or discrete dimeric cages. The addition of Cp_2Co^+ whose size is roughly at the limit of the open cavities results not only in a drastic change in the structural parameters (Table S2) of the constituent cages in comparison to Cage-1 but also to the formation of polymeric cages. The crystalline structural differences between PC-1 and PC-2 are also ascribed to the slight variations in the size and shape of these two cations (i.e., Cp_2Co^+ vs TEA^+; cf. Table S2). TEA^+ is too large to fit completely inside the open cavity and its alkyl substituents are too small to intrude appreciably into the voids in PC-1. As a result, the two face-to-face subunits of ligand 1 (i.e., colored the same in cage subunits A and B in Figure 2c) lie parallel to one another. The open cavity is also slightly compressed compared to that in PC-2 (Table S4).

The larger TBA^+ and DMV^{2+} cations are too large to be retained within the cage dimers and are found to lie outside the cavity. This change necessarily leads to a different location for the counter cations within the crystal structure Cage-1 containing DMA^+. The TBA^+ cation is even larger than TEA^+; however, its alkyl "arms" can intrude slightly into the cavity of Cage-3, which serves to orient the nearby cage subunits. Finally, DMV^{2+} is not only relatively large, it also bears two positive charges, and as mentioned above, this cation resides between two neighboring cage dimers and remains outside the cavity of Cage-5.

Morphological Control over the Self-assembly of Cages Based on Ligand 1. The choice of ancillary organic cations not only determines the chemical and crystalline structures of the cages produced from pyridine dipyrrolate and $Zn(acac)_2$ but also affects their higher order self-assembly behavior. As originally produced, Cage-1 displays little evidence of either cage−cage interactions in the solid state (Figure S4) or significant further self-assembly in solution.[12] In contrast, Cage-3, produced in the presence of TBA^+, is characterized by larger voids[15] (Figure S18 and Table S4) and a greater level of presumed π−π interactions between neighboring cage units. This leads to the formation of self-assembled particles with an average size of around 40 nm, as inferred from SEM observations (Figure 3a). Different behavior is seen in the case of Cage-5; this system forms 1D assemblies that are apparently stabilized by π−π interactions between the electron-deficient DMV^{2+} cations and the electron-rich ligand bridge between two neighboring cage dimers (Figure S19). These 1D assemblies interact further with surrounding solvent molecules (i.e., DMF and H_2O) to produce 2D layered assemblies (Figures S12 and S14) as inferred from the SEM analyses (Figure 3d). When TEA^+ and Cp_2Co^+ are used, the polymeric cages PC-1 and PC-2 that are

DOI: 10.1021/jacs.9b01042
J. Am. Chem. Soc. 2019, 141, 4749−4755

presumably formed initially aggregate into 1D fiber-like assemblies (Figure 3c,d). Thus, both the size and the charge play key roles in determining the initial cage structure and the morphologies of the assembled superstructures.

CONCLUSIONS

In conclusion, a set of very different cage products, including dimers (Cage-3 and Cage-5) and polymeric assemblies (made up of PC-1 and PC-2), have been successfully produced in a controlled manner from the same two starting materials, namely, the angular ligand 1 and $Zn(acac)_2$, in the presence of different ancillary organic cations (i.e., TBA^+, DMV^{2+}, TEA^+, and Cp_2Co^+, respectively). With the involvement of solvent molecules, these organic cations can serve as specific templates to control the cage structure. They also act to modulate further the assembly of individual cages, allowing formation of multidimensional ensembles. For instance, the polymeric cages PC-1 and PC-2 aggregate into 1D linear assemblies. In contrast, the dimeric cages, Cage-3 and Cage-5, pack in an orderly fashion to form particles and 2D layered assemblies, respectively. The finding that formally nonconstituent species, added organic cations in the present instance, can be used to fine-tune the multidimensional morphologies of assembled inorganic cages points the way toward a new approach to controlling the features of nanomaterials.

ASSOCIATED CONTENT

* Supporting Information

The Supporting Information is available free of charge on the ACS Publications website at DOI: 10.1021/jacs.9b01042.

Detailed crystallographic, experimental, and data for Cage-3, Cage-5, PC-1, and PC-2, calculated voids, ^{1}H NMR, UV−vis, and fluorescent spectral data (PDF)

Crystal data for Cage-3 (CIF)

Crystal data for Cage-5 (CIF)

Crystal data for PC-1 (CIF)

Crystal data for PC-2 (CIF)

AUTHOR INFORMATION

Corresponding Authors

*zhanghuacheng@utexas.edu

*sessler@cm.utexas.edu

ORCID

James T. Brewster, II: 0000-0002-4579-8074

Jonathan L. Sessler: 0000-0002-9576-1325

Notes

The authors declare no competing financial interest.

ACKNOWLEDGMENTS

The work was financially supported by the National Science Foundation (CHE-1807152) and the Robert A. Welch Foundation (F-0018). H.Z. would like to thank the "Young Talent Support Plan" of Xi'an Jiaotong University and the "Thousand Talents Program" of Shaanxi Province, China for finacial support.

REFERENCES

(1) (a) Hussain, F.; Hojjati, M.; Okamoto, M.; Gorga, R. E. Polymer-matrix nanocomposites, processing, manufacturing, and application: an overview. J. Compos. Mater. 2006, 40, 1511. (b) Liu, X.; Wang, D.; Li, Y. Synthesis and catalytic properties of bimetallic nanomaterials with various architectures. Nano Today 2012, 7, 448. (c) Khalil, M.; Jan, B. M.; Tong, C. W.; Berawi, M. A. Advanced nanomaterials in oil and gas industry: design, application and challenges. Appl. Energy 2017, 191, 287.

(2) (a) Guo, D.; Xie, G.; Luo, J. Mechanical properties of nanoparticles: basics and applications. J. Phys. D: Appl. Phys. 2014, 47, 013001. (b) Xie, W.; Guo, Z.; Gao, Q.; Wang, D.; Liaw, B.; Cai, Q.; Sun, X.; Wang, X.; Zhao, Li. Shape-, size- and structure-controlled synthesis and biocompatibility of iron oxide nanoparticles for magnetic theranostics. Theranostics 2018, 8, 3284.

(3) (a) Charitidis, C. A.; Georgiou, P.; Koklioti, M. A.; Trompeta, A. F.; Markakis, V. Manufacturing nanomaterials: from research to industry. Manufacturing Rev. 2014, 1, 11. (b) Wang, K.; Qi, D.; Li, Y.; Wang, T.; Liu, H.; Jiang, J. Tetrapyrrole macrocycle based conjugated two-dimensional mesoporous polymers and covalent organic frameworks: from synthesis to material applications. Coord. Chem. Rev. 2019, 378, 188.

(4) (a) Kim, Y.; Koo, J.; Hwang, I.; Mukhopadhyay, R.; Hong, S.; Yoo, J.; Dar, A. A.; Kim, I.; Moon, D.; Shin, T. J.; Ko, Y. H.; Kim, K. Rational design and construction of hierarchical superstructures using shape-persistent organic cages: porphyrin box-based metallosupramolecular assemblies. J. Am. Chem. Soc. 2018, 140, 14547. (b) Sun, Y.; Zhang, F.; Jiang, S.; Wang, Z.; Ni, R.; Wang, H.; Zhou, W.; Li, X.; Stang, P. J. Assembly of metallacages into solid superstructures with dimensions of up to micrometers and the formation of composite materials. J. Am. Chem. Soc. 2018, 140, 17297.

(5) (a) Service, R. F. How far can we push chemical self-assembly. Science 2005, 309, 5731. (b) Ozin, G. A.; Hou, K.; Lotsch, B. V.; Cademartiri, L.; Puzzo, D. P.; Scotognella, F.; Ghadimi, A.; Thomson, J. Nanofabrication by self-assembly. Mater. Today 2009, 12, 12. (c) Li, H.; Zhang, H.; Lammer, A. D.; Wang, M.; Li, X.; Lynch, V. M.; Sessler, J. L. Quantitative self-assembly of a purely organic three-dimensional catenane in water. Nat. Chem. 2015, 7, 1003. (d) Zhang, H.; Liu, Z.; Zhao, Y. Pillararene-based self-assembled amphiphiles. Chem. Soc. Rev. 2018, 47, 5491.

(6) (a) Inokuma, Y.; Yoshioka, S.; Ariyoshi, J.; Arai, T.; Hitora, Y.; Takada, K.; Matsunaga, S.; Rissanen, K.; Fujita, M. X-ray analysis on the nanogram to microgram scale using porous complexes. Nature 2013, 495, 461. (b) de Ruiter, G.; Lahav, M.; van der Boom, M. E. Pyridine Coordination chemistry for molecular assemblies on surfaces. Acc. Chem. Res. 2014, 47, 3407. (c) Cook, T. R.; Stang, P. J. Recent developments in the preparation and chemistry of metallacycles and metallacages via coordination. Chem. Rev. 2015, 115, 7001. (d) Chakraborty, S.; Newkome, G. Terpyridine-based metallosupramolecular constructs: tailored monomers to precise 2D-Motifs and 3D-metallocages. Chem. Soc. Rev. 2018, 47, 3991.

(7) (a) Shankar, S.; Balgley, R.; Lahav, M.; Popovitz-Biro, R.; Cohen, S. R.; van der Boom, M. E. Metal−organic microstructures: from rectangular to stellated and interpenetrating polyhedra. J. Am. Chem. Soc. 2015, 137, 226. (b) Zhang, D.; Ronson, T. K.; Nitschke, J. R. Functional capsules via subcomponent self-assembly. Acc. Chem. Res. 2018, 51, 2423.

(8) (a) Shankar, S.; Lahav, M.; van der Boom, M. E. Coordination-based molecular assemblies as electrochromic materials: ultra-high switching stability and coloration efficiencies. J. Am. Chem. Soc. 2015, 137, 4050. (b) Rizzuto, F. J.; Wu, W.-Y.; Ronson, T. K.; Nitschke, J. R. Peripheral templation generates an $Fe^{II}_8L_4$ guest-binding capsule. Angew. Chem. Int. Ed. 2016, 55, 7958. (c) McConnell, A. J.; Haynes, C. J. E.; Grommet, A. B.; Aitchison, C. M.; Guillemet, J.; Mikutis, S.; Nitschke, J. R. Orthogonal stimuli trigger self-assembly and phase transfer of $Fe^{II}_4L_4$ cages and cargoes. J. Am. Chem. Soc. 2018, 140, 16952.

(9) (a) Furutani, Y.; Kandori, H.; Kawano, M.; Nakabayashi, K.; Yoshizawa, M.; Fujita, M. In situ spectroscopic, electrochemical, and theoretical studies of the photoinduced host−guest electron transfer that precedes unusual host-mediated alkane photooxidation. J. Am. Chem. Soc. 2009, 131, 4764. (b) García-Simón, C.; Garcia-Borràs, M.; Gómez, L.; Parella, T.; Osuna, S.; Juanhuix, J.; Imaz, I.; Maspoch, D.; Costas, M.; Ribas, X. Sponge-like molecular cage for purification of

DOI: 10.1021/jacs.9b01042
J. Am. Chem. Soc. 2019, 141, 4749−4755

fullerenes. Nat. Commun. 2014, 5, 5557. (c) Zhang, H.; Zou, R.; Zhao, Y. Macrocycle-based metal-organic frameworks. Coord. Chem. Rev. 2015, 292, 74. (d) Rizzuto, F. J.; Wood, D. M.; Ronson, T. K.; Nitschke, J. R. Tuning the redox properties of fullerene clusters within a metal−organic capsule. J. Am. Chem. Soc. 2017, 139, 11008.
(10) (a) Fiedler, D.; Pagliero, D.; Brumaghim, J. L.; Bergman, R. G.; Raymond, K. N. Encapsulation of cationic ruthenium complexes into a chiral self-assembled cage. Inorg. Chem. 2004, 43, 846. (b) Custelcean, R. Anion encapsulation and dynamics in self-assembled coordination cages. Chem. Soc. Rev. 2014, 43, 1813. (c) Yang, D.; Zhao, J.; Yu, L.; Lin, X.; Zhang, W.; Ma, H.; Gogoll, A.; Zhang, Z.; Wang, Y.; Yang, X. J.; Wu, B. Air- and light-stable P_4 and As_4 within an anion-coordination-based tetrahedral cage. Angew. Chem. Soc. 2017, 139, 5946.
(11) (a) van der Boom, M. E.; Milstein, D. Cyclometalated phosphine-based pincer complexes: mechanistic insight in catalysis, coordination, and bond activation. Chem. Rev. 2003, 103, 1759. (b) Brumaghim, J. L.; Michels, M.; Raymond, K. N. Hydrophobic chemistry in aqueous solution: stabilization and stereoselective encapsulation of phosphonium guests in a supramolecular host. Eur. J. Org. Chem. 2004, 2004, 4552. (c) Gera, R.; Das, A.; Jha, A.; Dasgupta, J. Light-induced proton-coupled electron transfer inside a nanocage. J. Am. Chem. Soc. 2014, 136, 15909. (d) Wang, S.; Gao, X.; Hang, X.; Zhu, X.; Han, H.; Li, X.; Liao, W.; Chen, W. Calixarene-based $\{Ni_{18}\}$ coordination wheel: highly efficient electrocatalyst for the glucose oxidation and template for the homogenous cluster fabrication. J. Am. Chem. Soc. 2018, 140, 6271. (e) Trickett, C. A.; Osborn Popp, T. M.; Su, J.; Yan, C.; Weisberg, J.; Huq, A.; Urban, P.; Jiang, J.; Kalmutzki, M. J.; Liu, Q.; Baek, J.; Head-Gordon, M. P.; Somorjai, G. A.; Reimer, J. A.; Yaghi, O. M. Identification of the strong Brønsted acid site in a metal−organic framework solid acid catalyst. Nat. Chem. 2019, 11, 170.
(12) (a) Zhang, H.; Lee, J.; Lammer, A. D.; Chi, X.; Brewster, J. T.; Lynch, V. M.; Li, H.; Zhang, Z.; Sessler, J. L. Self-assembled pyridine-dipyrrolate cages. J. Am. Chem. Soc. 2016, 138, 4573. (b) McPherson, J. N.; Das, B.; Colbran, S. B. Tridentate pyridine−pyrrolide chelate ligands: an under-appreciated ligand set with an immensely promising coordination chemistry. Coord. Chem. Rev. 2018, 375, 285.
(13) Sakaida, S.; Otsubo, K.; Sakata, O.; Song, C.; Fujiwara, A.; Takata, M.; Kitagawa, H. Crystalline coordination framework endowed with dynamic gate-opening behaviour by being downsized to a thin film. Nat. Chem. 2016, 8, 377.
(14) Chen, L.; Reiss, P. S.; Chong, S. Y.; Holden, D.; Jelfs, K. E.; Hasell, T.; Little, M. A.; Kewley, A.; Briggs, M. E.; Stephenson, A.; Thomas, K. M.; Armstrong, J. A.; Bell, J.; Busto, J.; Noel, R.; Liu, J.; Strachan, D. M.; Thallapally, P. K.; Cooper, A. I. Separation of rare gases and chiral molecules by selective binding in porous organic cages. Nat. Mater. 2014, 13, 954.
(15) Hartlieb, K. J.; Holcroft, J. M.; Moghadam, P. Z.; Vermeulen, N. A.; Algaradah, M. M.; Nassar, M. S.; Botros, Y. Y.; Snurr, R. Q.; Stoddart, J. F. CD-MOF: a versatile separation medium. J. Am. Chem. Soc. 2016, 138, 2292.

DOI: 10.1021/jacs.9b01042
J. Am. Chem. Soc. 2019, 141, 4749−4755